Preparation and Adhesion of a Dual-Component Self-Assembled Dual-Layer Film on Silicon by a Dip-Coating Nanoparticles Method

Yufei Mo[†,‡] **and Mingwu Bai***[,†]

State Key Laboratory of Solid Lubrication, Lanzhou Institute of Chemical Physics, Chinese Academy of Sciences, Lanzhou 730000, People's Republic of China, and Graduate School of the Chinese Academy of Sciences, Beijing 100039, People's Republic of China

Received: March 26, 2008; Revised Manuscript Received: May 7, 2008

A novel microfabrication method is presented to fabricate with spatial control a dual-component self-assembled dual-layer film on silicon by dip-coating nanoparticles. In this research, the same chain length carboxylic acids with a fluorocarbon backbone chain and hydrocarbon backbone chain were composite-prepared on 3-aminopropyltriethoxysilane (APS) self-assembled monolayer (SAM). Film wettability was determined by measurement of contact angle, and thickness was determined with the ellipsometric method. Changes in adhesive properties of the film are determined by atomic force microscopy (AFM).

1. Introduction

Lubrication plays an important role in the micromechanical system (MEMS) just as it does for large mechanical machines. However, limited types of lubrication are available for MEMS due to their small size and close spacing of the components.[1] The class of materials known as self-assembled monolayers (SAMs) are organic molecular films spontaneously formed on certain materials with ordered conformation.[2] SAMs, which are typically formed by the adsorption of alkanethiols onto gold surfaces, or by the adsorption of alkylsilanes onto silica surfaces, have attracted widespread interest in a range of applications including fundamental studies of interfacial phenomena, such as wetting[3–5] and biological interaction,[6] and development of novel functional molecular thin film architectures.[7] Recently, SAMs as ideal molecular lubricants for MEMS have been given great attention because they solve the friction problem.[8] Alkylthiols, alkanoic acids, and alkylsilanes, which are produced on gold and silicon surfaces, respectively, are the most popular systems to be used for this purpose.[9–13] However, finding optimum lubricants for the MEMS continues to be a challenge in the field of nanotechnology. Investigation into the tribological behavior of SAMs derived from alkylsilanes has been an active topic, and it is imperative to find better lubricants for MEMS with longer durability and better tribological performance.[14–16]

SAMs have good rupture properties due to their strong bonding to substrate surfaces. They are expected not to migrate freely on the surface of the substrate. However, some molecules from SAMs may transfer to the surface of the pair when external force is applied to the contacting surface.[17] Because of the monolayer structure and flexibility, SAMs exhibit poor antiwear durability.[18–20] To utilize SAMs as lubricants to protect MEMS, it is necessary to consider the molecular layer structure as well as the strongly bonded characteristics of the lubricant.[21] To minimize interfacial energy, SAMs with low surface energy (e.g., perfluorinated *n*-alkanoic acid, $C_nH_{2n-1}O_2H$) are applied on the aluminum surfaces of the digital micromirror devices (DMD), which are used to reduce friction during contact between the spring tip and the landing site.[22] Our previous results[14,23,24] indicate that the dual-layer structure can help to improve the film quality and enhance their durability and load-bearing capacity. Meanwhile, it is observed that a hydrogenated carboxylic acid dual-layer film exhibits better friction reduction but poorer durability compared to the perfluorinated carboxylic acids dual layer.

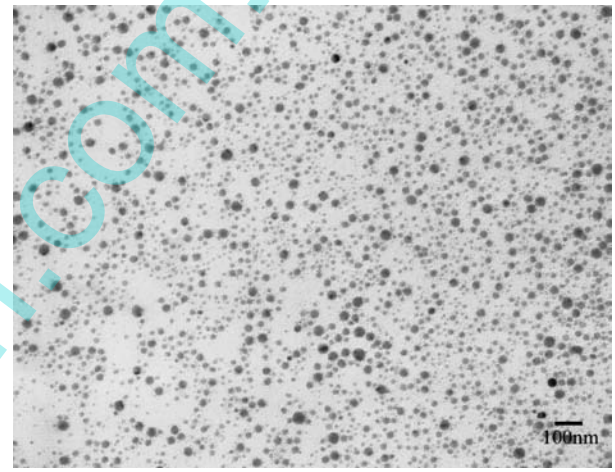

Figure 1. TEM image of Ag nanoparticles.

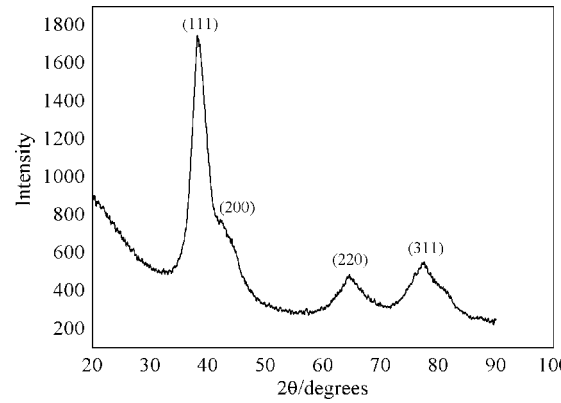

Figure 2. Typical XRD trace of Ag nanoparticles.

* Corresponding author. Tel: +86-931-4968080. Fax: +86-931-4968080. E-mail: mwbai@LZB.ac.cn.
† Lanzhou Institute of Chemical Physics.
‡ Graduate School of the Chinese Academy of Sciences.

10.1021/jp802608m CCC: $40.75
Published on Web 07/02/2008

SCHEME 1: Fabrication Process for the PFOA/STA−APS Dual-Component Dual-Layer Film[a]

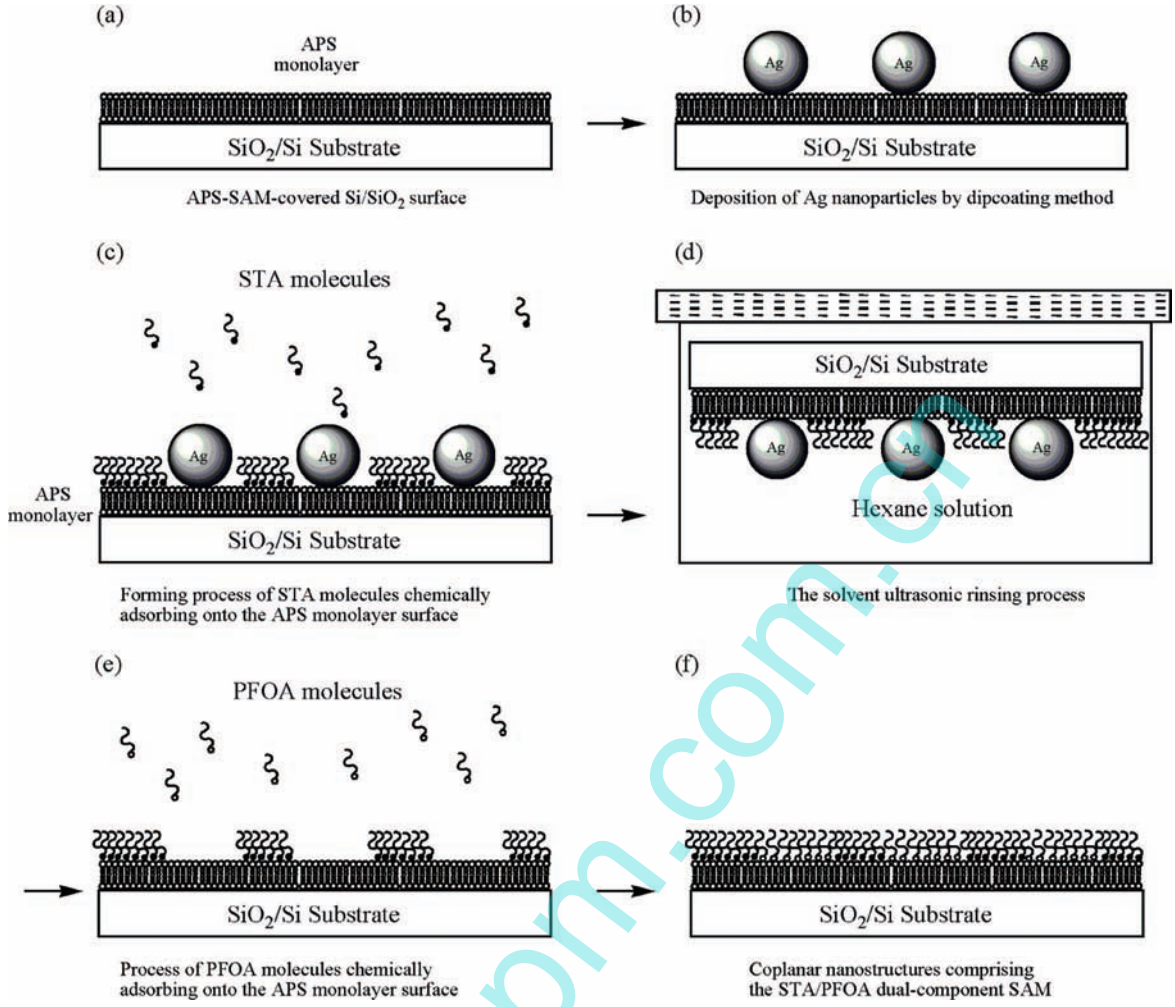

[a] (a) Formation of an APS monolayer on hydroxylated silicon substrate; (b) deposition of Ag nanoparticles by the dip-coating method; (c) formation process of STA molecules chemically adsorbing onto the Ag−APS monolayer surface; (d) process of Ag nanoparticles removal; (e) process of PFOA molecules filling in the pits of the film; (f) formation of the coplanar nanostructure STA/PFOA dual-component dual-layer film.

TABLE 1: Contact Angles and Thicknesses for the Silica Layer and the Modified Silicon Surfaces

test samples	water contact angle (deg)	thickness (nm)
SiO_2/Si	~0	~1.8
APS	44.0	0.7
STA/PFOA	108.0	2.0

Over the past years, the microfabrication of materials has attracted great interest for use in MEMS and other applications. Mixture component patterned surfaces offer a means for controlling the adhesive and wetting behavior of materials. This is important for a whole host of technological applications including cell growth,[25,26] protein manipulation,[27] and microfluidics.[28–31] According to previous reports, the mixture component structure can be fabricated by various techniques, including microcontact printing,[32–35] ultraviolet light,[36–38] electron beam,[39–41] and scanning probe microscope lithographies.[42–45] However, this microprocessing currently depends on complicated photolithographic technology, extremely high chemical durability, and physical stability. Furthermore, the area of the film is subject to mask or template restrictions. An alternative method requiring neither etching nor additional post treatments has been strongly demanded. Significant advancement has been made in nanoparticle research with synthetic techniques extending over a wide range of materials. However, as far as we know, nanoparticles being used as masks or templates has not been reported.

We designed a lubrication system consisting of dual-component self-assembled dual-layer films to minimize friction and a molecular mixture layer to prolong durability. In this paper, we report a novel strategy for a dual-component self-assembled film with control of spatial growth on a large surface area based on a dip-coating nanoparticles method. In selecting among the various SAMs, we particularly focus on the control of both fluorinated and hydrogenated backbone chain molecules because these molecules have strong potential applications in MEMS.

2. Experimental Section

2.1. Materials. Polished and cleaned single-crystal silicon wafer (P-type 100), obtained from GRINM Semiconductor Materials Co., Ltd., Beijing, was used as a substrate. The roughness of the wafer used was 0.18 nm. 3-Aminopropyltriethoxysilane (APS; 99%) was obtained from ACROS (New Jersey). Perfluorooctadecanoic acid (PFOA; 98%) was purchased from ABCR GmbH & Co. KG and used as received. Stearic acid (STA, 98%, Hushi Chemical Co., Ltd., Shanghai) was used as received.

2.2. Preparation and Characterization of Ag Nanoparticles. Monodisperse Ag nanoparticles capped by long-chain carboxylates were prepared with a method similar to that of ref 46, and their structure was characterized by transmission electron

SCHEME 2: Chemical Structure and Forming Process of STA and PFOA Molecules Chemically Adsorbing onto the APS Monolayer Surface

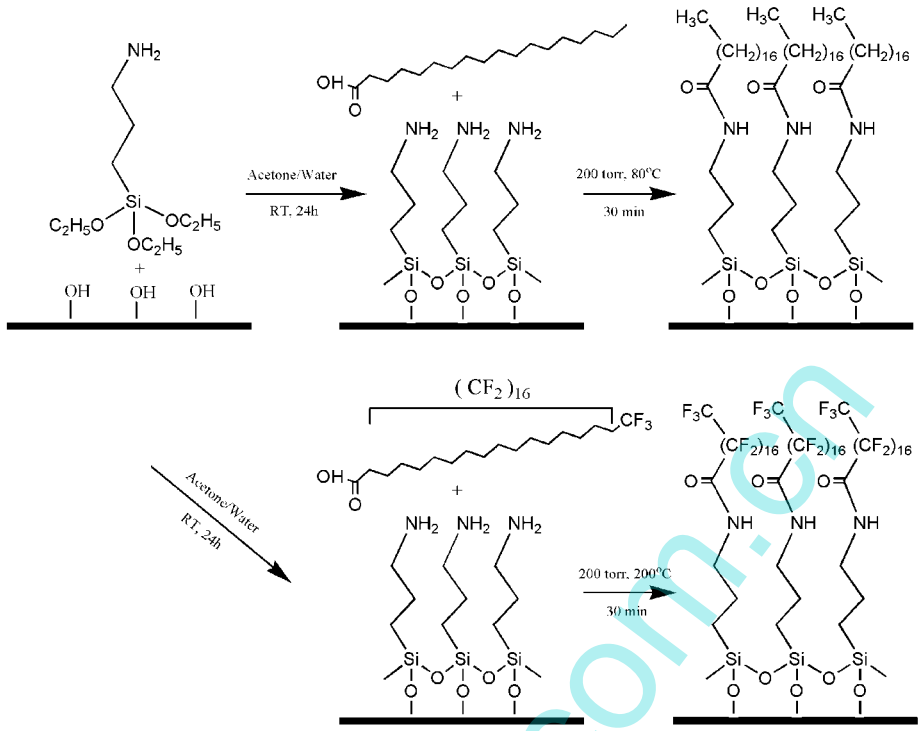

microscopy (TEM) and X-ray diffraction (XRD). In the preparation process, 3.0 g of silver stearate (Ag n-$C_{17}C_{35}COO$) was placed in a 100 mL round-bottomed flask with a magnetic stirrer, 50 mL of triethylamine was added, and then the reaction solution was stirred at 80 °C for 2 h. After cooling to room temperature, 20 mL of acetone was added to the solution to produce the precipitate, which was collected by filtration, washed with a small amount of acetone, and dried under vacuum. A TEM image (Figure 1) shows that the diameter of spherical nanoparticles was about 30−50 nm and the prepared nanoparticles slightly agglomerated. The Ag nanoparticles capped by long-chain carboxylates were highly soluble in nonpolar and weakly polar organic solvents such as toluene, chloroform, liquid paraffin, and hexane. Figure 2 gives the crystal structure of Ag nanoparticles examined by XRD. The diffraction peaks at $2\theta = 38.5°$, 45°, 65°, and 78° can be indexed to the (111), (200), (220), and (311) planes of face-centered cubic silver, respectively. The line broadening of the XRD peaks compared with that of bulk Ag material was primarily due to the size effect of small particles.

2.3. Pretreatment of Silicon Wafers. Silicon wafers were cleaned and hydroxylated by immersing them in piranha solution, a mixture of 7:3 (v/v) 98% H_2SO_4 and 30% H_2O_2, at 90 °C for 30 min. The modified Si substrates were ultrasonicated with isopropyl alcohol, ethanol, and acetone in turn to remove other physically adsorbed ions and molecules. The substrates were then dried with a nitrogen flow. The substrates were then placed into the APS solution of 5.0×10^{-3} M in a mixed solvent of acetone and ultrapure water (v/v = 5:1) and held for 24 h. The target monolayer of APS was thus formed on the hydroxylated silicon substrate. After rinsing with ultrapure water, the amino-terminated silicon substrate was prepared by self-assembly of APS.

2.4. Preparation of the Dual-Component Dual-Layer Film. A dual-component dual-layer film was formed according the process illustrated in Scheme 1a−f. As illustrated in Scheme 1a, an APS SAM was first formed on hydroxylated silicon substrate. The APS−SAM-covered Si/SiO_2 surface became relatively hydrophobic with a water contact angle of 44°. The APS−SAM-covered silicon substrate was then nanopatterned by dip-coating Ag nanoparticles hexane solution, as shown in Scheme 1b. After the solvent evaporated, the Ag nanoparticles arranged onto the APS-modified silicon surface. The dried samples were placed in a 100 mL sealed vessel with a glass container filled with 0.2 mL of STA precursor liquid. There was no direct contact between liquid and samples. The vessel was put into an oven maintained at a pressure of 200 Torr and temperature of 80 °C for 30 min. The STA molecules chemisorbed onto the APS-modified silicon surface with acidamide reaction by the chemical vapor deposition (CVD) method under vacuum, as shown in Scheme 1c. After being cooled in a desiccator, an STA monolayer was produced on the top of the APS monolayer. The cooled film samples were then ultrasonicated in hexane and acetone in turn to remove the Ag nanoparticles and the physisorbed STA molecules. The forming process is shown in Scheme 1d. After being dried with a nitrogen flow, the samples were placed in a 100 mL sealed vessel with a glass container filled with 0.2 mL of PFOA precursor liquid. The vessel was put into an oven maintained at a pressure of 200 Torr and temperature of 200 °C for 30 min, as shown in Scheme 1e. The PFOA molecules chemisorbed onto the exposed APS surface with acidamide reaction during the CVD process. After this, each sample was ultrasonically rinsed with isopropyl alcohol, acetone, and deionized water in turn to remove physisorbed ions and molecules. The samples were then dried with a nitrogen flow. The coplanar nanostructure comprising the STA/PFOA dual-component dual-layer SAM was successfully formed on the APS-modified silicon surface, as shown in Scheme 1f.

2.5. Characterization of the Dual-Component Dual-Layer Film. The static contact angles for ultrapure water on the films were measured with a Kyowa contact angle measurement

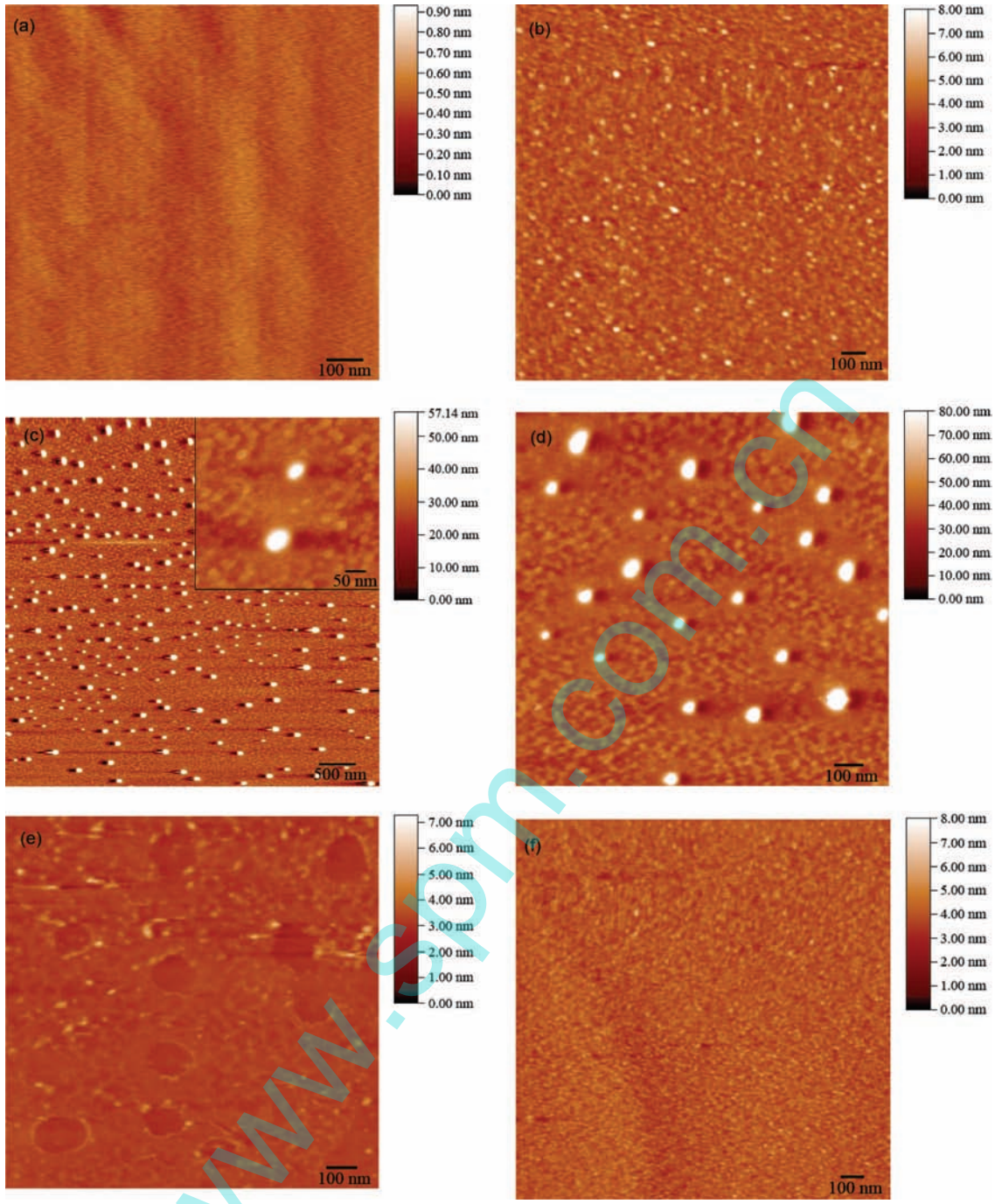

Figure 3. AFM images of the film surface. (a) Hydroxylated silicon surface. (b) Film surface of APS. (c) Ag nanoparticles arranged onto the film surface of APS. (d) STA layer formed on the Ag−APS-modified silicon surface. (e) Film surface after Ag removal. (f) Surface morphology of the STA/PFOA dual-layer film.

apparatus. At least five replicate measurements were carried out for each specimen, and the measurement error was below 2°.

The thicknesses of the films were measured on a Gaertner L116-E ellipsometer, which was equipped with a He−Ne laser (632.8 nm) set at an incident angle of 50°. A real reflective index of 1.40 was set for all the films. Five replicate measurements were carried out for each specimen, and the thicknesses were recorded to an accuracy of ±0.3 nm.

The chemical composition and structure of the surface were examined with a PHI-5702 multitechnique X-ray photoelectron spectrometer (XPS), using a pass energy of 29.35 eV, an excitation source of Mg Kα radiation ($h\nu$ = 1253.6 eV), and takeoff angle of 35°. The chamber pressure was about 3×10^{-8} Torr under the tested condition. The binding energy of contaminate carbon (C1s: 284.8 eV) was used as a reference.

A CSPM4000 atomic force microscope (AFM) with tapping mode was used to observe the film morphology. The adhesion of the film was characterized with an AFM/FFM controlled by CSPM4000 electronics, using the contact mode. A commercially available rectangle Si_3N_4 cantilever and back side coated by gold with a normal force constant, 0.4 N/m, and a Si_3N_4 tip with a radius of less than 10 nm (Budgetsensors Instruments Inc.) were employed. For all measurements the same cantilever was successfully used in this comparative study. Furthermore, to avoid the influence of molecules which may transfer to the tip on the AFM/FFM experiment, the tip was scanned on a

SCHEME 3: Illustration of the Convolution Effect between Tip and Ag Nanoparticles

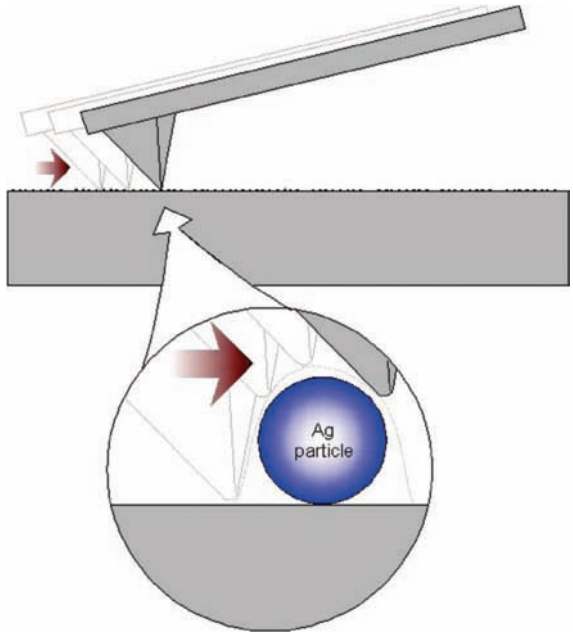

cleaved mica surface to remove these physically adsorbed molecules. The force distance curves were recorded, and the pull off force reckoned as the adhesive force, which was given by

$$F = K_c Z_p \quad (1)$$

where K_c is the force constant of the cantilever and Z_p is the vertical displacement of the piezotube, i.e., the deflection of the cantilever.[47,48] In data processing, a test of 10 measurements was made for each sample; repeated measurements were within 5% of the average value for each series.

3. Results and Discussion

Measurement of the static contact angle is an effective way to measure the variation of the chemical composition of solid surfaces. The contact angles for water and ellipsometric thicknesses on the hydroxylated silicon surface, APS, and STA/PFOA dual-component films are shown in Table 1. Naturally, the hydroxylated silicon surface and APS film are hydrophilic, with water contact angles of about 0° and 44.0°, respectively, which agree well with what has been reported.[49,50] Once the dual-component film formed on the APS monolayer, the contact angle greatly increased to 108.0°, and the resulting dual-component film surface became hydrophobic. The film thicknesses also gained increases to about 0.7 and 2.0 nm on the APS and STA/PFOA films, respectively. The variation of contact angles and thicknesses indicates that STA/PFOA molecules have successfully adsorbed onto the APS-coated surface. The APS monolayer with a terminal amino group is ready to make the acidamide reaction with the carboxylic acid under test conditions. On the basis of the covalent amide bond between the STA/PFOA and APS molecules, the reaction process is schematically shown in Scheme 2.

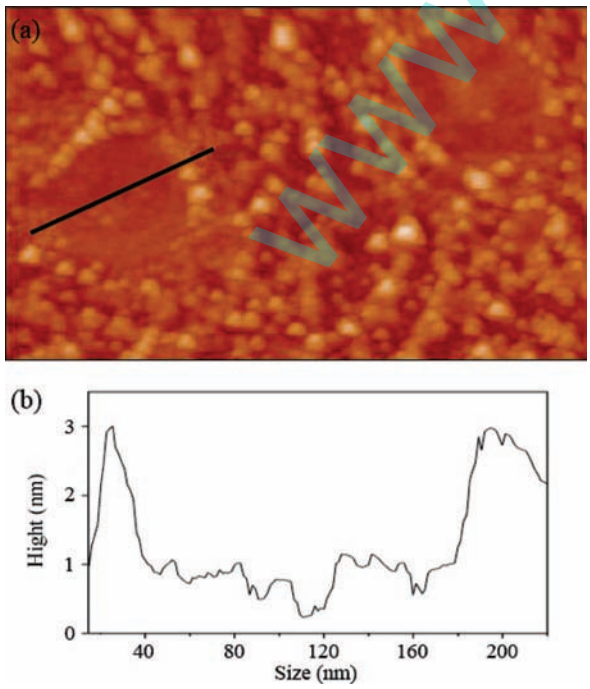

Figure 4. AFM image (a) and cross-sectional map (b) of pits.

SCHEME 4: Illustration of the Forming Process of the Pits[a]

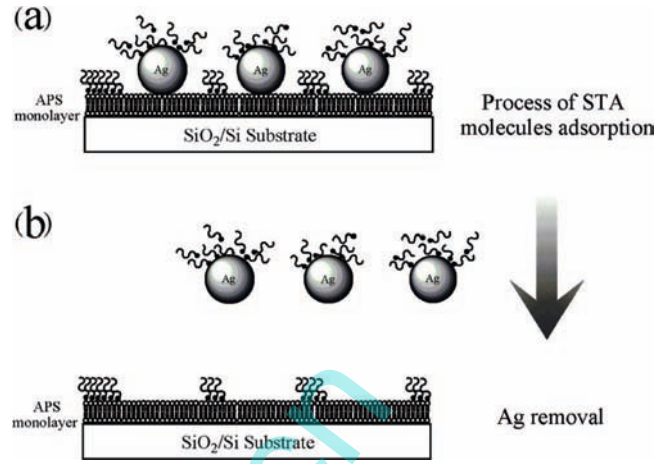

[a] (a) Process of STA molecules deposition; (b) process of Ag nanoparticles removal.

The geometric structure of the modified silicon was evaluated by AFM imaging. As shown in Figure 3a, the silicon surface was smooth, clean, and has microroughness of root-mean-square (rms) about 0.1 nm after the hydroxylation and cleaning process. An APS layer was first formed on silicon as amino-terminated Si substrates. From Figure 3b, the APS film was homogeneous and dense; it regularly distributed on the substrate with a microroughness of rms about 0.5 nm. To fabricate a dual-layer film, the APS layer covered silicon substrate was first nanopatterned by dip-coating Ag nanoparticles in hexane solution. After the solvent evaporated, Ag nanoparticles were arranged onto the APS film surface, as shown in Figure 3c. From the inset, a typical AFM image can be seen of Ag nanopattern on APS−SAM, in which grains corresponded to Ag nanoparticles. A difference of the diameter between Figures 1 and 3c can be observed; this discrepancy of measured size of nanoparticles results from the interaction of the tip shape with the surface topography (Scheme 3) and aggregation of nanoparticles in the solvent volatilization process during dip-coating. When cooled in nitrogen, the STA molecules absorbed onto the APS-modified silicon surface after the CVD process, as shown in Figure 3d. After Ag removal, it was observed that some pits appear at the film surface, as shown in Figure 3e. The pits corresponded to the region of removal of Ag nanoparticles. The surfaces of the bottom of the pits were the exposed APS layer surface. After

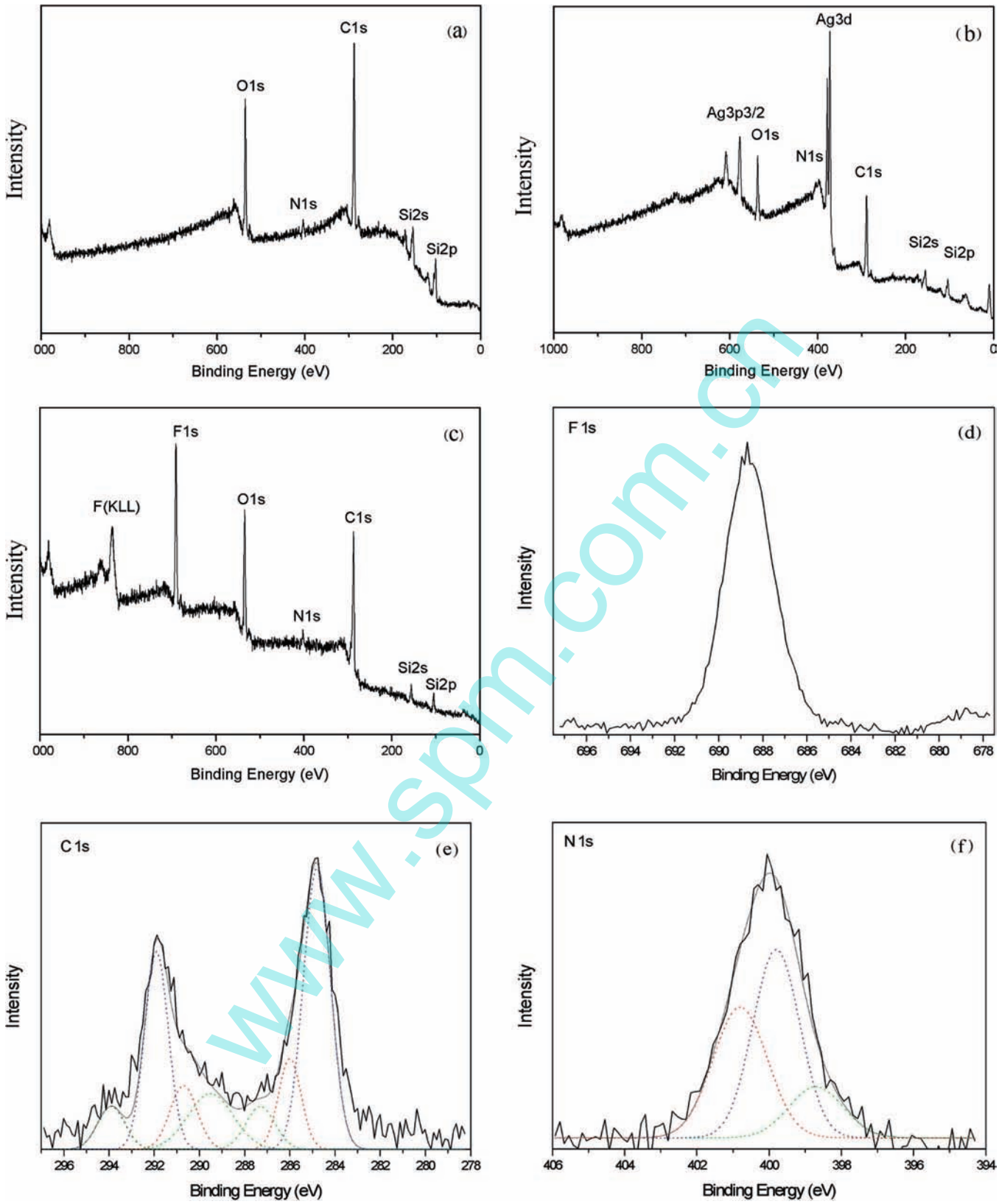

Figure 5. X-ray photoelectron survey spectra of (a) APS film, (b) Ag−STA/APS film, (c) PFOA/STA−APS film. (d) F1s, (e) C1s, and (f) N1s regions of a PFOA/STA−APS film.

PFOA molecules adsorbed onto the exposed amino groups of the APS layer, the film surface became relatively smooth and homogeneous (Figure 3f).

To observe these pits in more detail, the scanning area was narrowed, and the result is shown in Figure 4a, with the cross-sectional image in Figure 4b. From Figure 4b the mean height and diameter of pits were averaged at about 1.9 and 160 nm, respectively. The height of the pits agreed well with the thickness of the STA/PFOA layer (Table 1). An interesting result was observed in the AFM images that the diameter of the pits is greater than the diameter of the grains. We believe that the difference of diameter between the grains and pits was probably

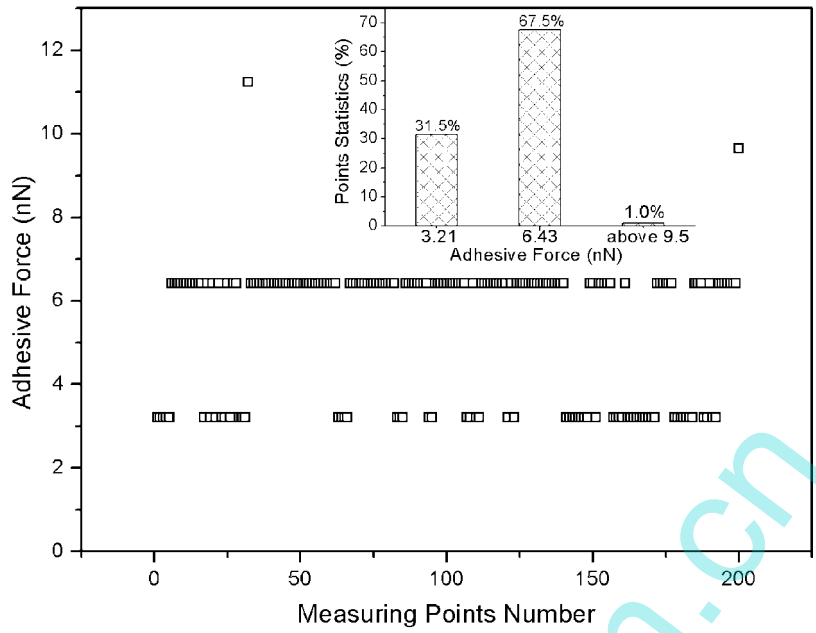

Figure 6. Plot of adhesion force and statistical distribution for the PFOA/STA−APS film (20 °C, 15% RH).

due to the following two reasons. First, as shown in Scheme 4, STA molecules adsorbed on the surface of nanoparticles and formed cross-linked molecules, so they inhibited other STA molecules deposited directly onto the nearby of Ag nanoparticles. The STA molecules adsorbed onto the spherical surface of Ag nanoparticles during the forming process of the STA layer (Scheme 4a) and were removed with Ag nanoparticles during the solvent rinsing process (Scheme 4b). Second, the adsorbed STA molecules around nanoparticles were less ordered and bonded around nanoparticles, and STA molecules of the outer region were chemically adsorbed and homogeneously distributed. This is partly supported by the observation from Figure 3d that the region near nanoparticles is different from other areas.

The surface chemical composition of the dual-component dual-layer films was determined by XPS. In this paper, we focused on the forming process of the dual-component dual-layer film. Figure 5 shows the XPS survey spectra of film surfaces at the main process. Figure 5a displays the spectrum obtained from the APS layer. Data show that there is no silver and fluorine on the silicon surface before deposition. Parts b and c of Figure 5 show the survey spectra of film surfaces before and after Ag removal and the PFOA deposition process, respectively. The XPS survey spectrum of the film surface (Figure 5b) shows four elements: carbon (C1s), oxygen (O1s), nitrogen (N1s), silicon (Si1s, Si2p), and silver (Ag3d, Ag3p3/2). No peaks related to Ag species appear in the XPS spectrum (Figure 5c). It means that Ag nanoparticles capped by long-chain carboxylates were removed completely by the hexane ultrasonic rinsing process. There were two additional peaks arising from the XPS survey spectrum, as shown Figure 5c. These peaks (F1s, F_{kll}) can be assigned to F atoms. While a single highly symmetrical peak of 688.4 eV appeared in the F1s spectrum (Figure 5d), seven peaks were observed in the C1s spectrum as shown in Figure 5e. The first peak at 284.8 eV is assigned to the $-CH_2-$ group in STA and APS, whereas the second peak at 286.0 eV might originate from the C atoms bonded to the N atoms (O═C−N−C*).[51] The third peak at 287.4 eV can be attributed to the carboxyl C atom (O═C*−N−C) in STA.[51] The forth and fifth peaks at 289.4 and 290.6 eV come from the carboxyl C atom (O═C*−N−C) and C atoms bonded to the N atoms (O═C−N−C*) in PFOA, respectively.[52] The sixth and seventh peaks at 292.1 and 293.9 eV are assigned to the $-CF_2-$ and $-CF_3$ groups in PFOA, respectively.[52,53] The above assignments clearly indicate that the STA/PFOA layer was formed on the APS-modified silicon surface with chemical reaction. The N1s spectrum that is shown in Figure 5f further supports this conclusion. There are three peaks of 398.7, 399.8, and 400.7 eV arising from the N1s spectrum. While the peak at 398.7 eV is assigned to the N atom in the amine group, the peak that appeared at 399.8 eV can be attributed to the N atom bonded to the carboxyl group (O═C−N*). The peak at 400.7 eV can be assigned to H-bonded amino group.[51,54,55]

Figure 6 shows the spatial distribution of the dual-component film by adhesion statistic measurement. The adhesive forces of STA and PFOA SAMs were measured as 3.21 and 6.43 nN, respectively. The adhesive force measurement was performed at a rate of 1 Hz along the scan axis and a scan size of 10 μm × 10 μm during scanning; at least 200 measuring points were carried out for each scan range. From the inset, it can be seen that the adhesive forces of the dual-component layer were calculated statistically as 31.5% and 67.5%. The surface coverage of the pits was calculated as a value of about 20% by using a post-treating software supplied by the AFM manufacturer, which approaches to surface coverage of the pits calculated from the data from the adhesive force measurement. The discrepancy between the surface coverage of pits and the statistical value of PFOA in the adhesion measurement is probably because some STA molecules comprising a SAM exchanged gradually when exposed to the PFOA atmosphere, which results from displacement of SAMs by exchange.[56–60]

4. Conclusions

We report a simple, versatile approach for fabricating coplanar dual-component dual-layer films. The experimental results show that the dual-layer film comprising a dual-component upper layer with hydrogenated and fluorinated backbone chains regulated the spatial growth on the APS underlayer. The mechanism of this site-selective growth can be explained as follows. An APS layer was first formed on hydroxylated silicon substrate. Monodisperse Ag nanoparticles capped by long-chain carboxy-

lates played a role in the effective suppression of undesired composite growth on sites. Due to acidamide reaction between STA and APS molecules, the STA molecules chemisorbed onto the APS-modified surface. The film surface fabricated lunar crater-like pits microstructure and amino-terminated surface exposed in the bottom of the pits after Ag nanoparticles removal. The PFOA molecules absorbed onto the exposed amino-terminated surface with acidamide reaction, and the pits of the film were occupied completely by PFOA molecules.

The interfacial functionalities of the dual-component dual-layer film presented here can be freely designed by selecting the appropriate carboxylic acid adsorbed on the amino-terminated surface to regulate the surface properties. Since our process demonstrated here focused on the area control of adhesion, friction, and wettability of the SAM-covered surface, we expect that this technique could be applied to various surfactant molecules such as organosilanes and thiols. In addition, our process is applicable for various substrates other than a silicon surface. In comparison with conventional methods reported thus far, the dual-component dual-layer process demonstrated here is simple and effective, allowing the fabrication of composite films on a large-scale area. We believe that this technique is potentially applicable for the fabrication of novel microstructure materials.

Acknowledgment. This work was funded by the Innovative Group Foundation from the National Natural Science Foundation of China (NSFC) under Grant No. 20773148, NSFC 50675217, and National 973 Program: 2007CB607601.

References and Notes

(1) Spearing, S. M. *Acta Mater.* **2000**, *48*, 179.
(2) Ulman, A. *An Introduction to Ultrathin Organic Films*; Academic: NewYork, 1991.
(3) Bain, D. C.; Evall, J.; Whitesides, G. M. *J. Am. Chem. Soc.* **1989**, *111*, 7155.
(4) Ralph, G. N.; Lawrence, H. D.; David, L. A. *J. Am. Chem. Soc.* **1990**, *112*, 558.
(5) Paul, E. L.; Ralph, G. N.; Whitesides, G. M. *J. Phys. Chem.* **1992**, *96*, 5097.
(6) Paul, A. D.; John, P. F.; Hans, A. B.; Ralph, H.; Gabriel, P. L.; Whitesides, G. M. *J. Am. Chem. Soc.* **1994**, *116*, 2225.
(7) Willner, I. ; Doron, A.; Katz, E.; Levi, S.; Frank, A. J. *Langmuir* **1996**, *12*, 946.
(8) Liu, H.; Ahmed, I. U.; Scherge, M. *Thin Solid Films* **2001**, *381*, 135.
(9) Touzov, I.; Gorman, C. B. *J. Phys. Chem. B* **1997**, *101*, 5263.
(10) Cha, K. H.; Kim, D. E. *Wear* **2001**, *251*, 1169.
(11) Clear, S. C.; Nealey, P. F. *Langmuir* **2001**, *17*, 720.
(12) Gautheir, S.; Aime, J. P.; Bouhacina, T.; Attias, A. J.; Desbat, B. *Langmuir* **1996**, *12*, 5126.
(13) Hutt, D. A.; Leggett, G. J. *Langmuir* **1997**, *13*, 2740.
(14) Ren, S. L.; Yang, S. R.; Zhao, Y. P. *Langmuir* **2003**, *19*, 2763.
(15) Choudross, M.; Grest, G. S.; Stevens, M. J. *Langmuir* **2002**, *18*, 8392.
(16) Eapen, K. C.; Patton, S. T.; Zabinski, J. S. *Tribol. Lett.* **2002**, *12*, 35.
(17) Ren, S.; Yang, S.; Zhao, Y.; Zhou, J.; Xu, T.; Liu, W. *Tribol. Lett.* **2002**, *13*, 233.
(18) Ruehe, J.; Novotny, V. J.; Kanazawa, K. K.; Clarke, T.; Street, G. B. *Langmuir* **1993**, *9*, 2383.
(19) Patton, S. T.; William, D. C.; Eapen, K. C.; Zabinski, J. S. *Tribol. Lett.* **2000**, *9*, 199.
(20) Rye, R. R.; Nelson, G. C.; Dugger, M. T. *Langmuir* **1997**, *13*, 2965.
(21) Hsu, S. M. *Tribol. Int.* **2004**, *37*, 537.
(22) Bhushan, B. *Microelectron. Eng.* **2007**, *84*, 387.
(23) Ma, J. Q.; Liu, J. X.; Mo, Y. F.; Bai, M. W. *Colloids Surf., A* **2007**, *301*, 481.
(24) Ma, J. Q.; Pang, C. J.; Mo, Y. F.; Bai, M. W. *Wear* **2007**, *263*, 1000.
(25) Ito, Y. *Biomaterials* **1999**, *20*, 2333.
(26) Nygren, N. *Colloids Surf., B* **1996**, *6*, 329.
(27) Xu, Y.; Waston, T.; Bruening, M. L. *Anal. Chem.* **2003**, *75*, 185.
(28) Handique, K.; Bruke, D. T.; Mastrangelo, C. H.; Burns, M. A. *Anal. Chem.* **2000**, *72*, 4100.
(29) Huang, Z.; Wang, P. C.; Feng, J.; MacDiarmid, A. G.; Xia, Y.; Whitesides, G. M. *Synth. Met.* **1997**, *85*, 1375.
(30) Wojtyk, J. T. C.; Tomietto, M.; Boukherroub, R.; Wayner, D. D. M. *J. Am. Chem. Soc.* **2001**, *123*, 1535.
(31) Karthaus, O.; Grasjo, L.; Maruyama, N.; Shimomura, M. *Thin Solid Films* **1998**, *327*, 829.
(32) Kaumar, A.; Whitesides, G. M. *Appl. Phys. Lett.* **1993**, *63*, 2002.
(33) Kaumar, A.; Whitesides, G. M. *Science* **1994**, *263*, 60.
(34) Jeon, N. L.; Clem, P. G.; Payne, D. A.; Nuzzo, R. G. *Langmuir* **1996**, *12*, 5350.
(35) Xia, Y. N.; Whitesides, G. M. *Angew. Chem., Int. Ed.* **1998**, *37*, 551.
(36) Duleey, C. S.; Georger, L. H.; Krauthamer, J. V.; Stenger, D. A.; Fare, T. L.; Calvert, J. M. *Science* **1991**, *252*, 551.
(37) Brandow, S. L.; Chen, M. S.; Aggarwal, R.; Dulcey, C. S.; Calvert, J. M.; Dressick, W. J. *Langmuir* **1999**, *15*, 5429.
(38) Harnett, C. K.; Satyalakshmi, K. M.; Craighead, H. G. *Langmuir* **2001**, *17*, 178.
(39) Lercel, M. J.; Tiberio, R. C.; Chapman, P. F.; Craighead, H. G.; Sheen, C. W.; Parkin, A. N.; Allara, D. L. *J. Vac. Sci. Technol., B* **1993**, *11*, 2823.
(40) Mino, N.; Ozaki, S.; Ogawa, K.; Hatada, M. *Thin Solid Films* **1994**, *243*, 374.
(41) Hild, R.; David, C.; Muller, H. U.; Volkel, B.; Kayser, D. R.; Grunze, M. *Langmuir* **1998**, *14*, 342.
(42) Kim, Y. T.; Bard, A. J. *Langmuir* **1992**, *8*, 1096.
(43) Lercel, M. J.; Redinbo, G. F.; Craighead, H. G.; Sheen, C. W.; Allara, D. L. *Appl. Phys. Lett.* **1994**, *65*, 974.
(44) Perkins, F. K.; Dobisz, E. A.; Brandow, S. L.; Koloski, T. S.; Calvert, J. M.; Rhee, K. W.; Kasakowski, J. E.; Marrian, C. R. K. *J. Vac. Sci. Technol., B* **1994**, *12*, 3725.
(45) Kleineberg, U.; Brechling, A.; Sundermann, M.; Heinzmann, U. *Adv. Funct. Mater.* **2001**, *11*, 208.
(46) Yanmamoto, M.; Kashiwagi, Y.; Nakamoto, M. *Langmuir* **2006**, *22*, 8581.
(47) Xiao, X. D.; Qian, L. M. *Langmuir* **2000**, *16*, 8153.
(48) Tsukruk, V. V.; Bliznyuk, V. N. *Langmuir* **1998**, *14*, 446.
(49) Chen, K.; Caldwell, B.; Mirkin, C. A. *J. Am. Chem. Soc.* **1993**, *115*, 1193.
(50) Caldwell, W. B.; Chen, K.; Mirkin, C. A. *Langmuir* **1993**, *9*, 1945.
(51) Chance, J. J.; Purdy, W. C. *Langmuir* **1997**, *13*, 4487.
(52) Chen, P. J.; Wallace, R. M. *J. Vac. Sci. Technol., A* **1998**, *16*, 700.
(53) Sugimura, H.; Ushiyama, K.; Hozumi, A.; Talai, O. *J. Vac. Sci. Technol., B* **2002**, *20*, 393.
(54) Song, X. Y.; Zhai, J.; Wang, Y. L.; Jiang, L. *J. Colloid Interface Sci.* **2006**, *298*, 267.
(55) Peeling, J.; Hruska, F. E.; Mclntyrc, N. S. *Can. J. Chem.* **1978**, *56*, 1555.
(56) Fleming, M. S.; Walt, D. R. *Langmuir* **2001**, *17*, 4836.
(57) Love, J. C.; Estroff, L. A.; Kriebel, J. K.; Nuzzo, R. G.; Whitesides, G. M. *Chem. Rev.* **2005**, *105*, 1103.
(58) Laibinis, P. E.; Fox, M. A.; Folkers, J. P.; Whitesides, G. M. *Langmuir* **1991**, *7*, 3167.
(59) Schlenoff, J. B.; Li, M.; Ly, H. *J. Am. Chem. Soc.* **1995**, *117*, 12528.
(60) Shon, Y. S.; Lee, T. R. *J. Phys. Chem. B* **2000**, *104*, 8192.

JP802608M